Spring 2025

Transfection Of Ionizable Lipid Nanoparticles On Raw 264.7 And Mda-Mb-231

Lavanya Bhargava
Missouri University of Science and Technology

Department:

TRANSFECTION OF IONIZABLE LIPID NANOPARTICLES ON RAW 264.7 AND MDA-MB-231

by

LAVANYA BHARGAVA

A THESIS

Presented to the Graduate Faculty of the

MISSOURI UNIVERSITY OF SCIENCE AND TECHNOLOGY

In Partial Fulfillment of the Requirements for the Degree

MASTER OF SCIENCE IN CHEMICAL ENGINEERING

2024

Approved by:

Dr. Hu Yang, Advisor
Dr. Jee-Ching Wang
Dr. Hany El-Azab

ABSTRACT

This thesis investigates the preparation, characterization, and transfection efficiency of various ionizable lipid nanoparticles (LNPs) formulated for the delivery of mRNA encoding enhanced green fluorescent protein (EGFP) in RAW 264.7 macrophages and MDA-MB-231 breast cancer cell lines. The ionizable cationic lipid studied are ALC-035, C12-200, C14-4, PPZ-A10, DLin-MC3-DMA. The study addresses the need for effective gene delivery systems to provide a safe and versatile platform that protects and transports nucleic acids into target cells. LNPs were synthesized using microfluidic mixing methods, incorporating lipid components such as the cationic lipids, DSPE, DOPE, cholesterol and PEG lipids to achieve controlled particle sizes, encapsulation efficiencies, and stability profiles. Dynamic light scattering (DLS) characterized the LNPs immediately post-synthesis and after a seven-day storage period. Particle sizes ranged from 185.7 nm to 247.0 nm initially, with polydispersity index (PI) values between 0.19 and 0.31, indicating stable and uniform formulations. Over a seven-day period, average particle sizes showed less than 10% size increases. Zeta potential values remained close to neutral, between -1.238 mV and -1.786 mV, supporting sustained stability. The formulation was encapsulated across all formulations showing tr, as confirmed by gel electrophoresis. Transfection efficiency was evaluated using both fluorescence microscopy and flow cytometry. Both cell lines displayed significant expression 24 hours post-transfection with PPZ and C14. Flow cytometry analysis showed that PPZ, C14 formulations led to approximately 70% EGFP-positive cells in RAW 264.7 and 65% in MDA-MB-231, while. These results demonstrate the potential of LNPs as a robust mRNA delivery system, providing valuable insights into nanocarrier optimization for a variety of therapeutic applications especially in cancers.

ACKNOWLEDGMENTS

I would like to acknowledge and show my appreciation to my thesis advisor, Dr. Hu Yang for graciously accepting me into his group, and consistently encouraging and supporting me throughout my research. He always believed in me and taught me the skills for me to succeed as a graduate student. I am very fortunate to have worked under his expert guidance. I would also like to thank Dr. Jee-Ching Wang, and Dr. Hany Elazab for serving as my committee members. Secondly, I would like to thank the Missouri S&T Chemical Engineering Department for providing me knowledge and skill that I will need to succeed in my future opportunities. I would also like to extend a great appreciation to Vidit Singh, and my entire lab group for offering me continuous moral support and help me with everything.

Finally, I would like to express my greatest appreciation to my parents Sumeer and Shilpi, and my sister Sukanya Bhargava. They have always been my biggest supporters, and the greatest role models in teaching me how to succeed across all walks of life. Their motivation, encouragement, and love has been the largest driving force behind this achievement.

TABLE OF CONTENTS

Page

ABSTRACT iii

ACKNOWLEDGMENTS iv

LIST OF ILLUSTRATIONS viii

LIST OF TABLES x

1. INTRODUCTION 1

1.1. GENES AND PROTEINS AS THERAPEUTICS 1

1.2. GENE DELIVERY SYSTEM 1

1.2.1. Dendrimers. 3

1.2.2. Lipid Nanoparticles. 5

1.2.2.1. Lipsome. 5

1.2.2.2. Solid lipid nanoparticles (SLNs). 5

1.2.2.3. Cationic lipid nanoparticles. 5

1.2.2.4. Ionizable lipid nanoparticles 6

1.2.3. Characterization and Optimization of iLNPs. 9

1.3. BATCH AND CONTINUOUS SYNTHESIS METHODS 10

1.3.1. Batch Synthesis Methods. 10

1.3.2. Continuous Synthesis of Lipid Nanoparticles Using Microfluidic Methods. 13

1.3.3. Multi Inlet Vortex Mixing (MIVM). 14

1.3.4. Microfluidic Flow Focusing. 15

2. EXPERIMENTATION 17

2.1. IONIZABLE LIPID NANOPARTICLE PREPARATION 17
2.1.1. Materials. 17
2.1.2. Calculation for Lipid Quantities and concentration. 17
2.1.3. Procedure. 18
2.1.3.1. Preparation of Lipid Solution. 18
2.1.3.2. Preparation of Aqueous Phase. 18
2.1.3.3. Microfluidic Mixing. 18
2.1.3.4. Purification and Dialysis. 19
2.1.3.5. Characterization of Encapsulation Efficiency. 19
2.2. TRANSFECTIONS STUDIES 20
2.2.1. Cell Lines and Culture Conditions. 20
2.2.2. Procedure. 20
2.2.2.1. Cell Preparation. 20
2.2.2.2. Lipofectamine Complex Addition. 20
2.2.2.3. LNP formulation addition. 21
2.2.2.4. Transfection Process. 21
2.2.2.5. Post-Transfection Analysis. 21
3. RESULTS AND DISCUSSION 23
3.1. PARTICLE CHARACTERIZATION 23
3.2. ENCAPSULATION EFFECIENCY 25
3.3. TRANSFECTION RESULTS 26
3.3.1. Fluorescence Microscopy. 26
3.3.2. Flow Cytometry 29

4. CONCLUSION 32

APPENDIX 35

BIBLIOGRAPHY 36

VITA 39

LIST OF ILLUSTRATIONS

Page

Figure 1.1. Viral Vector Gene Delivery..... 3

Figure 1.2. Extracellular and intracellular barrier in mRNA delivery. 3

Figure 1.3. Dendrimer Structure. 4

Figure 1.4. Lipid based nanoparticle structure (created with BioRender.com). 6

Figure 1.5. N,N'-(piperazine-1,4-diylbis(propane-3,1-diyl))bis(3-(didecylamino)propanamide) or PPZ-A10. 8

Figure 1.6. [(4-Hydroxybutyl)azanediyl]di(hexane-6,1-diyl) bis(2-hexyldecanoate) or ALC-1035. 8

Figure 1.7. C14-494, Lipid B-4, Lipid B4 or C14-4. 9

Figure 1.8. D-Lin-MC3-DMA. 9

Figure 1.9. C12-200. 9

Figure 1.10. Schematic of T-junction mixing and Hydrodynamic flow focusing. 16

Figure 2.1. Schematic of Microfluidics Formation of LNP step. 19

Figure 3.1. Day 1 LNP size distribution. 24

Figure 3.2. Day 2 LNP size distribution. 25

Figure 3.3. Gel Electrophoresis of LNP formulations with RNA and DNA ladder. 26

Figure 3.4 Fluorescent image of RAWW cell line with lipofectamine formulation 27

Figure 3.5 Fluorescent image of RAW cell line with PPZ formulation 27

Figure 3.6 Fluorescent image of RAW cell line with C14 formulation..... 27

Figure 3.7 Fluorescent image of MDA-MB-231 cell line with C14 formulation..... 28

Figure 3.8 Fluorescent image of MDA-MB-231 cell line with PPZ formulation 28

Figure 3.9 Fluorescent image of MDA-MB-231 cell line with lipofectamine 28

Figure 3.10 Flow cytometer FITC-A channel graph for RAW cell line with C14-4, C12, and PPZ formulation respectively. 29

Figure 3.11. Flow cytometer FITC-A channel graph for MDA-MB-231 cell line with C14-4, PPZ, and lipofectamine formulation respectively..... 30

Figure 3.12 Flow cytometer transfection for MDA-MB-231 cell line with various formulations..... 30

Figure 3.13: Flow cytometer transfection for RAW cell line with various formulations. 31

LIST OF TABLES

Table Page

Table 2.1 Sample Material and Molar ratios for ALC-1035 18

Table 3.1. Day 1 of particle characterization 24

Table 3.2. Day 7 of particle characterization 24

1. INTRODUCTION

1.1. GENES AND PROTEINS AS THERAPEUTICS

Gene therapies and protein therapeutics are among the most advanced and promising approaches for treating a wide range of diseases, including cancer, cardiovascular disease, and immunodeficiencies. These therapies are not only central to the current drug market but also represent a transformative direction for biopharmaceuticals. Gene therapy seeks to introduce specific genetic material into target cells to either correct underlying genetic issues or slow disease progression (Cetin et al., 2024). This approach can involve replacing a disease-causing gene with a healthy version or inactivating malfunctioning genes. Examples of gene therapy products include plasmid DNA, mRNA, and patient-derived genes. Gene therapies represent a transformative direction for biopharmaceuticals, offering advanced approaches to treat a wide range of diseases, including cancer, cardiovascular disorders, and immunodeficiencies (Petrich et al., 2019)

One of the primary challenges in using genes and proteins as therapeutics is developing a delivery system that ensures these agents reach target cells effectively. This challenge is addressed by encapsulating gene and protein therapies in specialized delivery systems, designed to protect the therapeutic agents and facilitate their efficient transport into cells (Kumar et al., 2024)

1.2. GENE DELIVERY SYSTEM

Currently, viral-based platforms dominate as gene transfection vehicles in clinical gene therapy trials due to their high efficiency and specificity in delivering therapeutic genes into cells

(Minskaia et al., 2024). As shown in Figure 1.1 (Ju et al., 2018) these viral vectors, such as adenoviruses and lentiviruses, function by binding to specific cell surface receptors to enter the cell via endocytosis. Once inside, the viral capsid or envelope allows the plasmid carrying the therapeutic gene to escape the endosome—a crucial step known as endosomal escape. This process prevents the gene from being degraded within the acidic endosomal environment. After escaping the endosome, the viral vector directs the plasmid DNA towards the cell's nucleus, where it can be transcribed, leading to therapeutic protein production and gene expression (Ju et al., 2018)

However, viral vectors come with significant risks, such as potential immune responses, insertional mutagenesis, and manufacturing challenges, which limit their scalability and safety (Nayak et al., 2009). Consequently, there is a strong push toward developing non-viral delivery systems.

Non-viral approaches, including liposomes, lipid nanoparticles (LNPs), and dendrimers, offer alternative solutions with reduced immunogenicity and increased adaptability for large-scale production (Wang et al., 2022). These systems generally encapsulate the therapeutic gene material (e.g., plasmid DNA or mRNA) within a nanoparticle. Similarly to viral delivery, upon contact with the cell membrane, non-viral vectors enter cells mainly through endocytosis. Like viral vectors, achieving endosomal escape is crucial for effective gene delivery in non-viral methods. Non-viral vectors are often engineered with ionizable lipids or pH-sensitive components that enable endosomal destabilization, releasing the genetic material into the cytoplasm (Nayerossadat et al., 2012). Some of the extra and intracellular barriers are shown in Figure 1.2 (Mendonça et al., 2023)

Once in the cytoplasm, mRNA can be directly translated into protein, whereas plasmid DNA requires transport to the nucleus for transcription. Non-viral systems, particularly lipid

nanoparticles, thus rely heavily on optimized endosomal escape mechanisms to ensure efficient gene delivery and expression (Nayerossadat et al., 2012).

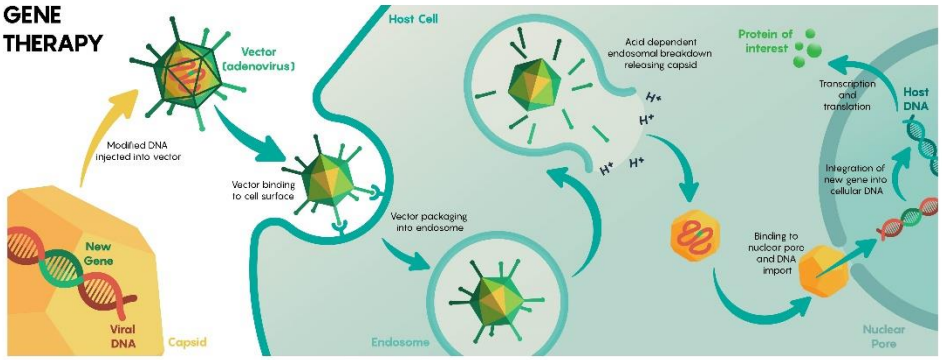

Figure 1.1. Viral Vector Gene Delivery.

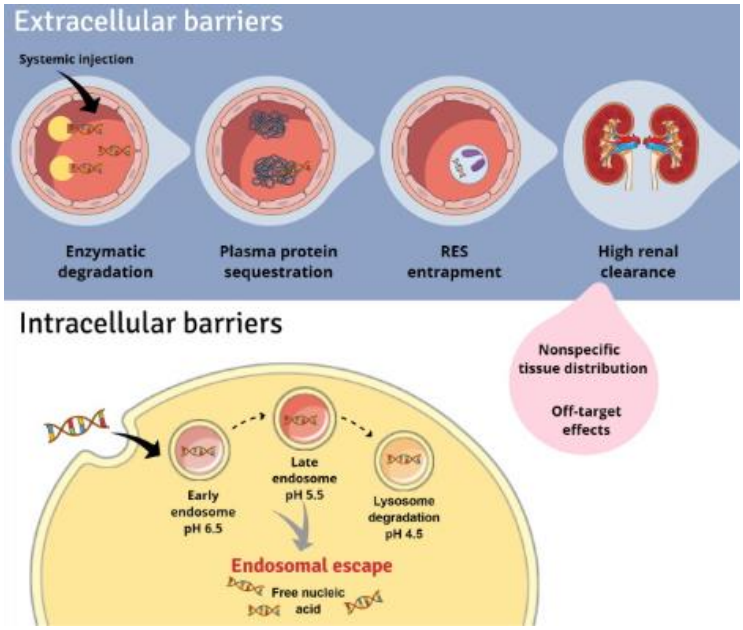

Figure 1.2. Extracellular and intracellular barrier in mRNA delivery.

1.2.1. Dendrimers. Dendrimers are polymer-based nanostructures with a symmetrical, branched design and a high density of functional end groups, making them

versatile for biomedical applications such as targeted drug delivery, gene and protein delivery, bioimaging, and enhanced therapeutic effectiveness (Sherje et al., 2018). Polyamidoamine (PAMAM) dendrimers, shown in Figure 1.3 (Carrión et al., 2023), possess primary amino groups on their surface that enable interaction with nucleic acids, condensing them into stable, protected particles (Berényi et al., 2014). PAMAM dendrimers also promote cellular uptake through endocytosis. However, higher generation dendrimers can be toxic to cells, a challenge often addressed by conjugating polyethylene glycol (PEG) to their surface, which also improves solubility. PEGylated dendrimers are preferred in biological applications as they enhance the structural stability of DNA-loaded complexes (Yang et al., 2006)). In protein therapy, dendrimers can be modified to interact with both cationic and anionic groups on protein surfaces. For instance, phenylboronic acid (PBA) can bind cationic amine and imidazole groups via nitrogen-boronate complexes, while amine groups on the dendrimer can conjugate with anionic sites on the protein (C. Liu et al., 2019).

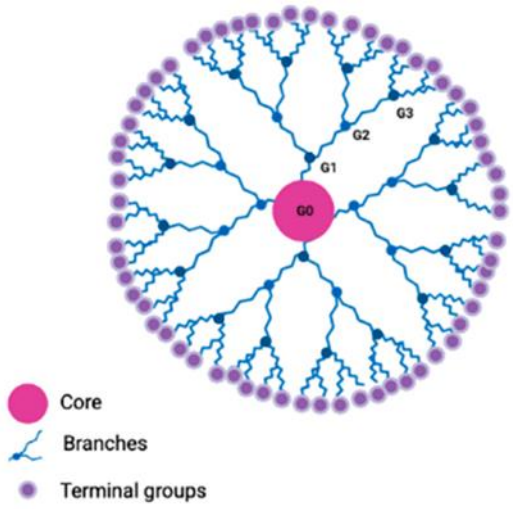

Figure 1.3. Dendrimer Structure.

1.2.2. Lipid Nanoparticles. Lipid-based nanocarriers, particularly lipid nanoparticles (LNPs) and ionizable lipid nanoparticles, have gained attention in drug delivery systems, especially in the delivery of nucleic acids such as siRNA, mRNA, and pDNA (Kumar et al., 2022). Due to their unique properties, including biocompatibility, encapsulation capabilities, and versatility (Liu et al., 2024).

Lipid nanoparticles protect therapeutic agents from metabolic degradation, enhancing bioavailability and reducing immunogenicity and systemic toxicity. Their membrane allows for the attachment of ligands, enabling targeted delivery to specific cells or tissues (Liu et al., 2024). These properties make LNPs suitable for applications ranging from chemotherapy and immunotherapy to vaccine delivery and gene therapy

1.2.2.1. Liposome. Liposomes are spherical vesicles as shown in Figure 1.4 with a lipid bilayer capable of encapsulating both hydrophilic and hydrophobic drugs. Due to their biocompatibility and potential for targeted delivery, they have been extensively researched for drug delivery applications (Nsairat et al., 2022). However, liposomes can suffer from stability issues, including rapid clearance from the bloodstream, which limits their efficacy in some cases (Giannopoulos-Dimitriou et al., 2024)

1.2.2.2. Solid lipid nanoparticles (SLNs). SLNs as shown in Figure 1.4 offer structural integrity and controlled release capabilities, making them suitable for lipophilic drugs. They utilize lipids in a solid state to encapsulate drugs (Akanda et al., 2023).

1.2.2.3. Cationic lipid nanoparticles. Cationic LNPs carry a positive charge, forming stable complexes with nucleic acids for effective encapsulation. However, they may present toxicity concerns due to their surface charge (Sun et al., 2023).

1.2.2.4. Ionizable lipid nanoparticles. Ionizable lipids as shown in Figure 1.4 used in LNPs remain neutral at physiological pH, becoming positively charged in acidic environments. This property is beneficial for endosomal escape, facilitating drug release (Tang et al., 2023).

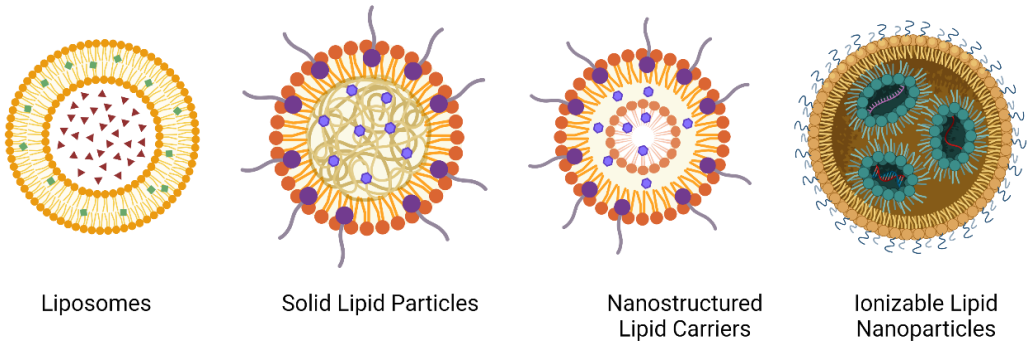

Figure 1.4. Lipid based nanoparticle structure (created with BioRender.com).

Applications of ionizable LNPs: An example is ALC-0315, which was the key component in Pfizer-BioNTech COVID 19 vaccine, takes on a positive charge in an acidic endosome environment, transitioning from a bilayer to an inverted hexagon phase to release its contents into the cytosol (Saadati et al., 2022). LNPs have been crucial in other applications in cancer immunotherapy and heart disease. C14-4 and AA3-DLIN, for instance, have been shown to effectively deliver siRNA for gene silencing in vitro and in vivo (Yonezawa et al., 2020).

Type of cationic lipids: The Ionizable lipids are critical components in lipid nanoparticles and provide the ionizable aspect to the LNP.

C12-200, as shown in Figure 1.9, is a polyamine ionizable lipid with a branched structure. It protonates in acidic environments, which enhances endosomal escape by

disrupting the membrane and allowing efficient transfection. C12-200 is recognized for its high transfection efficiency and low toxicity (Kauffman et al., 2015).

ALC-0315, as shown in Figure 1.6, is an ionizable lipid that shares a similar pH-responsive behavior to C12-200. It becomes positively charged in acidic conditions, improving cellular uptake and endosomal escape, while maintaining a neutral charge at physiological pH to minimize toxicity. This lipid has become an essential component in mRNA LNP formulations (Kauffman et al., 2015).

C14-4, as shown in Figure 1.7, is a PEGylated lipid known for its role in stabilizing LNPs and enhancing circulation time by reducing aggregation. Its short lipid chain allows rapid dissociation in the bloodstream, making it highly effective for targeted delivery, especially to the liver (Kauffman et al., 2015).

PPZ, as shown in Figure 1.5, is an ionizable lipid that enhances the stability of LNPs and their ability to escape from endosomes. It features a piperazine group that plays a critical role in the interaction with nucleic acids, facilitating efficient encapsulation and subsequent release within the cell. PPZ is particularly valuable in formulations requiring enhanced endosomal escape (Kauffman et al., 2015).

Dlin-MC3-DMA, as shown in Figure 1.8, is another well-established ionizable lipid, widely used in mRNA and siRNA formulations. It exhibits low toxicity and high delivery efficiency due to its ability to change charge in acidic environments, which is critical for facilitating the endosomal release of genetic material Kauffman et al., 2015).

A critical parameter in the design of LNPs is the nitrogen-to-phosphate (N to P ratio, which measures the molar ratio of the nitrogen groups in ionizable lipids to the phosphate groups in the encapsulated nucleic acids. This ratio significantly impacts the

electrostatic interactions within LNPs, influencing encapsulation efficiency and delivery performance. Optimal N to P ratios, typically ranging from 2:1 to 6:1, ensure robust encapsulation while minimizing cytotoxicity. Ratios that are too high-risk aggregation and toxicity, whereas suboptimal ratios may compromise delivery efficiency (Haque et al., 2024; Mendonça., 2023).

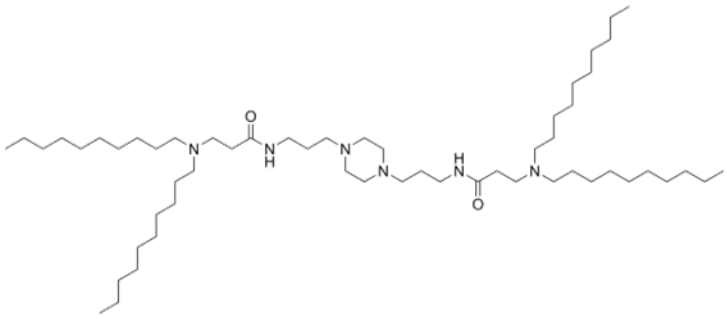

Figure 1.5. N,N'-(piperazine-1,4-diylbis(propane-3,1-diyl))bis(3-(didecylamino)propanamide) or PPZ-A10.

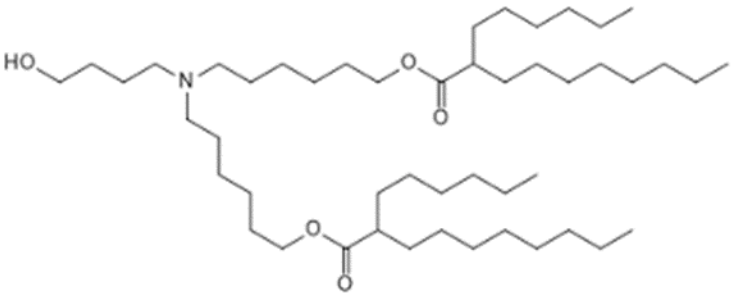

Figure 1.6. [(4-Hydroxybutyl)azanediyl]di(hexane-6,1-diyl) bis(2-hexyldecanoate) or ALC-1035.

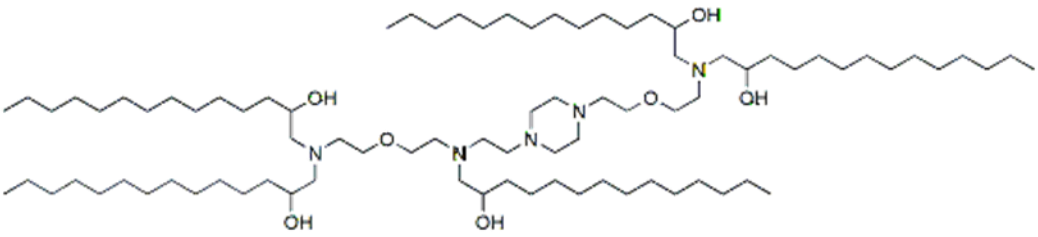

Figure 1.7. C14-494, Lipid B-4, Lipid B4 or C14-4.

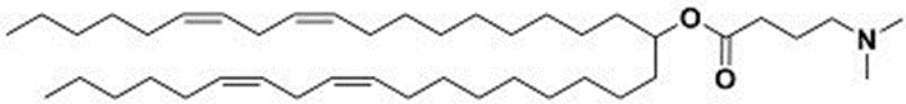

Figure 1.8. D-Lin-MC3-DMA.

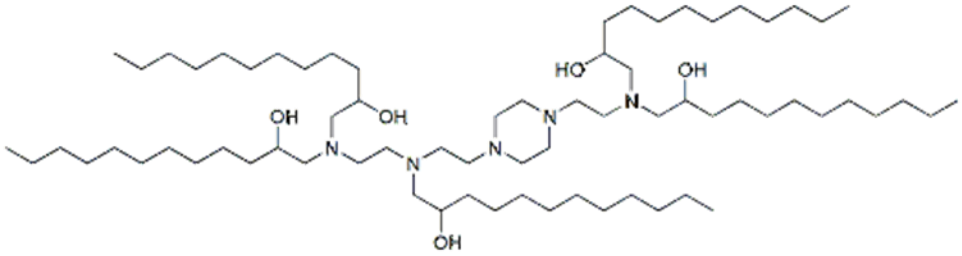

Figure 1.9. C12-200.

1.2.3. Characterization and Optimization of iLNPs. Generally, LNPs are composed of several key components:

- **Ionizable Cationic Lipids:** These lipids facilitate electrostatic binding with nucleic acids in acidic environments and release them in neutral environments (Mendonça et al., 2023).
- **Phospholipids:** These assist in stabilizing the lipid bilayer, improving LNP structure (Mendonça et al., 2023).

- **Cholesterol:** Cholesterol provides structural stability by intercalating into the lipid bilayer (Mendonça et al., 2023).
- **PEG-Lipid (Polyethylene Glycol-Lipid):** PEG-lipids prevent particle aggregation and prolong systemic circulation (Mendonça et al., 2023).
- **Helper Lipids:** aid cellular uptake and endosomal release. **DOPE** and **DSPC** are commonly used. DOPE promotes fusion with the endosomal membrane, bypassing the endosomal pathway, while DSPC forms a stable bilayer, enhancing LNP stability (Mendonça et al., 2023).

1.2.3.1. Characterization Techniques. DLS and gel electrophoresis are utilized to analyze LNP structure and size.

1.2.3.2. Size and Surface Charge. Particles of ~100 nm are often optimal for cellular uptake, balancing efficacy and stability. LNPs ranging from 20–200 nm with neutral or minimal surface charge reduce clearance by the reticuloendothelial system, thus prolonging circulation time (Augustine et al., 2020).

1.2.3.3. mRNA-LNP-Based Vaccines and Cancer Immunotherapy. mRNA-LNPs are used in prophylactic vaccines and are tested in cancer trials to induce an immune response within tumors. Examples include mRNA-LNPs encoding cytokines like IL-12, IL-15, and IL-36γ, which activate TH1 cells in the tumor microenvironment (Wang et al., 2024).

1.3. BATCH AND CONTINUOUS SYNTHESIS METHODS

1.3.1. Batch Synthesis Methods. Batch synthesis methods are widely used for laboratory-scale production of lipid nanoparticles (LNPs) due to their straightforward

setup and adaptability to different lipid compositions. These methods are essential for early-phase development, as they allow researchers to explore and optimize nanoparticle properties such as particle size, encapsulation efficiency, and stability. Below are three common batch synthesis techniques: extrusion, thin-film hydration, and freeze-drying.

1.3.1.1. Extrusion Method. The extrusion method is a batch technique that involves forcing a lipid suspension through membranes with defined pore sizes to achieve uniform nanoparticle size and distribution. This approach is particularly effective for reducing particle size and generating unilamellar vesicles from multilamellar lipid structures. Lipid nanoparticles are first formed through a preliminary method, such as thin-film hydration (described below). The resulting lipid suspension typically contains multilamellar vesicles (MLVs) with a wide range of particle sizes. The suspension is then extruded through polycarbonate membranes with controlled pore sizes (e.g., 100 nm), reducing the vesicles to unilamellar structures and narrowing the particle size distribution. Multiple passes through the membrane ensure consistent size reduction and improve uniformity. Extrusion is often performed at elevated temperatures, just above the phase transition temperature of the lipids, to ensure the lipids remain in a flexible state and are easy to shape. Extrusion allows precise control over particle size, making it suitable for applications requiring high uniformity, such as drug delivery systems where size consistency is crucial for biodistribution and cellular uptake. It is relatively simple and can be scaled up for larger batch production. This method requires specialized equipment and is time-consuming, as multiple extrusions may be necessary to achieve the desired size distribution. Additionally, some lipid compositions may be susceptible to degradation or shear stress during extrusion.

1.3.1.2. Thin-Film Hydration (Bangham Method). Thin-film hydration, also known as the Bangham method, is one of the most used techniques for producing lipid nanoparticles, especially for encapsulating hydrophilic drugs within the aqueous core or hydrophobic drugs within the lipid bilayer.

This method involves creating a dry lipid film, which is then hydrated with an aqueous solution. Lipids are first dissolved in an organic solvent, such as chloroform or methanol, and deposited in a round-bottom flask. The solvent is evaporated, typically under vacuum, to form a thin lipid film on the inner surface of the flask. Once the solvent is removed, an aqueous solution (often containing the drug or nucleic acid payload) is added to the flask (Xiang et al., 2017)

Upon hydration, the lipids spontaneously assemble into multi-lamellar vesicles (MLVs). Hydration temperature and agitation during this process play essential roles in controlling the efficiency of particle formation and the encapsulation of the payload. Often, MLVs formed by thin-film hydration are further processed by extrusion or sonication to achieve uniform, smaller particles. Thin-film hydration allows for the formation of LNPs with a high encapsulation efficiency and is suitable for a variety of payloads. It is adaptable for small-scale production and can be further optimized to include additional processing steps (e.g., extrusion) to improve particle uniformity. The method often produces a broad particle size distribution, and the vesicles may require further processing to achieve the desired size range for specific applications. Additionally, batch-to-batch consistency can be challenging to maintain (Hope et al., 1986; Evers et al., 2018).

1.3.1.3. Freeze-Drying (Lyophilization). In freeze-drying, an LNP suspension is first frozen, typically at -80°C or lower, to lock the particles in place. The frozen suspension is then subjected to a high vacuum, allowing the frozen water to sublimate directly from ice to vapor, bypassing the liquid phase (Ward et al., 2020). This process removes the aqueous content, leaving a dry powder of lipid nanoparticles.

To prevent particle aggregation or structural collapse during freeze-drying, cryoprotectants (e.g., sucrose or trehalose) are often added to the suspension before freezing. Freeze-drying greatly enhances the stability and shelf life of LNPs, making them more practical for storage and transportation. The dry powder form can be reconstituted with minimal loss of particle integrity, which is especially beneficial for formulations intended for clinical use or long-term storage. Freeze-drying requires specialized equipment and the addition of cryoprotectants, which must be optimized to avoid altering the LNP properties. Without proper cryoprotectants, freeze-drying may lead to particle aggregation or morphological changes upon rehydration (Trenkenschuh et al., 2021; Ward et al., 2020).

1.3.2. Continuous Synthesis of Lipid Nanoparticles Using Microfluidic Methods. Continuous synthesis methods for lipid nanoparticles (LNPs) have become essential for ensuring reproducibility, scalability, and control over particle properties. Among these, Microfluidic Vortex Mixing (MIVM) and Microfluidics Flow Focusing are two advanced techniques that leverage precise control of fluid flow to create uniform nanoparticles. These methods are highly effective for the large-scale production of LNPs used in gene therapy, vaccine delivery, and other therapeutic applications.

1.3.2.1. Multi Inlet Vortex Mixing (MIVM). Microfluidic Vortex Mixing (MIVM) is a widely used continuous synthesis method that relies on vortex-induced mixing within a microfluidic device. This approach is particularly advantageous for generating highly uniform LNPs with narrow size distributions. In MIVM, lipid-containing organic solutions (such as ethanol) are introduced through a central inlet, while the aqueous phase (often an acetate buffer containing mRNA or other payloads) is injected through side inlets at controlled flow rates. When the two streams meet, the vortex created by the fluid dynamics at the intersection leads to rapid mixing, enabling consistent nanoparticle formation. MIVM allows precise control over LNP size by adjusting flow rates and phase concentrations. The vortex mixing mechanism creates nanoparticles quickly, minimizing the risk of particle aggregation and achieving high encapsulation efficiency. MIVM is particularly effective for forming LNPs between 50-150 nm, a size range ideal for cellular uptake and systemic delivery (Carugo et al., 2016). While MIVM offers excellent control, it requires careful optimization of flow parameters to avoid excessive shear forces, which can compromise nanoparticle integrity or damage sensitive payloads like mRNA. Additionally, scaling up requires either parallel microfluidic channels or integration into a larger flow system, which can be technically challenging (Liu et al., 2008; Zhang et al., 2019).

1.3.2.2. Microfluidic Flow Focusing. Microfluidic Flow Focusing, as shown in Figure 1.10 (Lopes et al., 2022), is another technique that achieves continuous LNP synthesis by confining the lipid phase into a focused stream within the aqueous phase. This method typically involves a central channel for the lipid solution flanked by two channels for the aqueous solution, creating a narrow “focused” lipid stream. The controlled interaction between the phases allows for precise control over particle size and uniformity (Jürgens et al., 2023).

In microfluidic flow focusing, the main mixing mechanism is laminar flow, where the aqueous phase compresses the lipid stream into a narrow region, enhancing diffusion-based mixing. This setup reduces shear and promotes homogeneous particle formation. Flow rates of the aqueous and lipid phases are optimized to maintain the focused stream and prevent agglomeration or premature nucleation (Jiang et al., 2014).

Flow focusing offers high reproducibility and the ability to produce LNPs with a narrow size distribution, which is crucial for applications that require batch-to-batch consistency, such as vaccine production. It also supports the encapsulation of delicate payloads, as the controlled mixing process reduces mechanical stress (Maeki et al., 2023).

Both MIVM and Microfluidic Flow Focusing provide efficient, scalable, and reproducible solutions for LNP synthesis. They are especially beneficial for applications that demand high-quality nanoparticle production with consistent size and encapsulation characteristics, making them ideal for clinical and industrial applications.

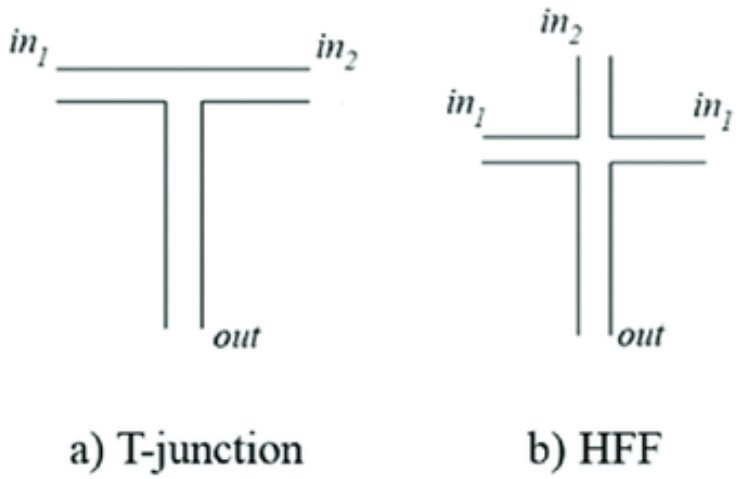

Figure 1.10. Schematic of T-junction mixing and Hydrodynamic flow focusing.

2. EXPERIMENTATION

2.1. IONIZABLE LIPID NANOPARTICLE PREPARATION

2.1.1. Materials. The following are the materials used for the preparation of the lipid nanoparticles:

- Lipid Components: DSPE-PEG-Mannose (3.4k), DOPE-PEG-Mannose (2k), ionizable cationic lipids such as ALC
- Buffers and Solvents: Acetate buffer (pH ~5.0), phosphate-buffered saline (PBS), ethanol.
- Nucleic Acids: EGFP mRNA
- Microfluidics Device: For mixing organic and aqueous phases.
- 10 kDa Dialysis Tubes in PBS with magnetic stirrer
- Gel Electrophoresis Setup: For assessing encapsulation efficiency.

2.1.2. Calculation for Lipid Quantities and concentration. Using molecular weights and the desired lipid composition, calculate the mass of each lipid component needed per batch as shown in the calculation shown in Appendix, and the sample ratios are shown in Table 2.1.

Table 2.1 Sample Material and Molar ratios for ALC-1035

Material	**Molar ratio**
DOPE	10
Cholesterol	38.5
PEG 2000	1.5
Ionizable Cationic Lipid	50

2.1.3. Procedure. A schematic is shown in Figure 2.1 (Singh 2023).

2.1.3.1. Preparation of Lipid Solution. Dissolve each lipid component (DSPE-PEG-Mannose, DOPE-PEG-Mannose, cationic lipids, cholesterol, and PEG-lipids) in ethanol. Mix thoroughly to achieve a homogeneous organic phase.

2.1.3.2. Preparation of Aqueous Phase. Dilute the mRNA in acetate buffer at pH ~5.0. The buffer facilitates mRNA-lipid interaction and assists in achieving the desired N to P ratio of 6:1 ratio by maintaining a stable charge environment for encapsulation.

2.1.3.3. Microfluidic Mixing. The procedure is outlined below.

a. Using a microfluidics device, combine the ethanol-lipid mixture with the mRNA-acetate buffer solution.

b. Set the flow rates at a 1:3 ratio to achieve rapid mixing, typically with the aqueous phase at a higher flow rate than the organic phase. This promotes controlled nanoparticle formation and consistent size.

c. The process leads to spontaneous self-assembly of LNPs as the ethanol dilutes in the aqueous phase, encapsulating the mRNA within the ionizable lipid core.

2.1.3.4. Purification and Dialysis. The procedure is outlined before.

d. After LNP formation, subject the solution to dialysis against PBS to remove residual ethanol and unencapsulated mRNA. Dialysis tubing with a molecular weight cutoff (MWCO) of 10-12 kDa is used for 12-24 hours, with buffer changes every 4 hours.

e. Ensure isotonic conditions by adding PBS, which maintains particle stability and prepares the solution for downstream applications.

2.1.3.5. Characterization of Encapsulation Efficiency. Perform gel electrophoresis on a small aliquot of the dialyzed LNP sample to assess encapsulation efficiency. The encapsulated mRNA should not migrate significantly on the gel, whereas free mRNA will migrate, indicating non-encapsulated mRNA.

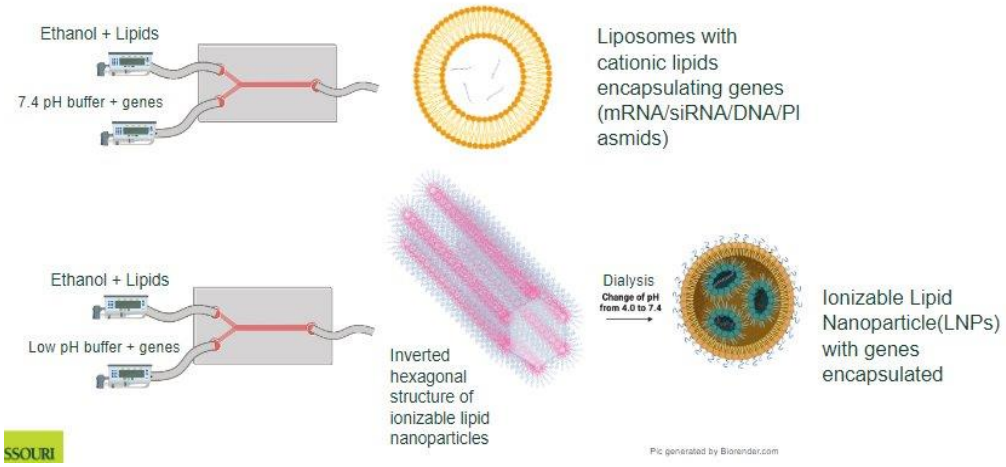

Figure 2.1. Schematic of Microfluidics Formation of LNP step.

2.2. TRANSFECTIONS STUDIES

2.2.1. Cell Lines and Culture Conditions. The cell lines used are RAW 264.7 macrophages and MDA-MB-231 breast cancer cells. Both cell lines were maintained in standard cell culture conditions (37°C, 5% CO_2) in DMEM supplemented with 10% fetal bovine serum (FBS) and 1% penicillin-streptomycin.

2.2.2. Procedure. The procedure is outlined below.

2.2.2.1. Cell Preparation. The procedure is outline below:

- Cells were grown in T75 flasks to reach approximately 75% confluence.
- RAW 264.7 cells (80,000 cells per well) and MDA-MB-231 cells (50,000 cells per well) were seeded in 24-well plates.
- After seeding, plates were incubated for 24 hours to allow cell attachment and recovery.

2.2.2.2. Lipofectamine Complex Addition. To form Lipofectamine-nucleic acid complexes, Lipofectamine 2000 (Thermo Fisher Scientific) was used according to the manufacturer's instructions. Briefly, Lipofectamine was diluted and incubated with the desired amount of mRNA for complex formation. The mRNA was added to the Lipofectamine reagent, and the mixture was incubated for 20 minutes at room temperature to allow the nucleic acid to be encapsulated within the lipid nanoparticles. The Lipofectamine-mRNA complexes were then applied to each well containing adherent cells, ensuring the final concentration of mRNA in each well was 0.5 μg.

2.2.2.3. LNP formulation addition. The LNP formulation was optimized to encapsulate the specified amount of mRNA (0.5 μg) per well. This formulation, including ionizable lipids such as C12-200, ALC-0315, and additional helper lipids, ensures efficient mRNA encapsulation and enhances transfection efficiency. The amount of LNP formulation added was calculated based on the encapsulation capacity and required dose of mRNA, ensuring that the final volume delivered a precise quantity of mRNA. This precise formulation ensures effective delivery while minimizing the potential toxicity of excess lipid content.

2.2.2.4. Transfection Process. The procedure is outlined below:

- **Cell Starvation**: Prior to adding LNPs, cells were starved in serum-free DMEM for 4 hours to enhance transfection efficiency by promoting cell uptake.
- **Addition of LNP-mRNA Complex**: After starvation, the LNP-mRNA complexes were added directly to the wells containing cells in serum-free media.
- **Incubation**: Cells were incubated with the LNPs for 4-6 hours at 37°C. After this incubation, the media was replaced with fresh DMEM containing 10% FBS, and cells were cultured overnight.

2.2.2.5. Post-Transfection Analysis. The procedure outlined is for after the cells are harvested after 24 hours which was done by a fluorescent microscope and a flow cytometer.

Fluorescence microscopy: Transfection efficiency was initially assessed using fluorescence microscopy. Cells were imaged to visualize EGFP expression, with

transfected cells exhibiting green fluorescence indicative of successful mRNA delivery and expression.

Flow cytometry: Quantitative analysis of transfection efficiency was conducted using flow cytometry. Cells were washed with PBS, trypsinized, and resuspended in PBS for flow cytometry analysis. A minimum of 10,000 events per sample was collected, and the percentage of EGFP-positive cells was calculated to determine transfection efficiency.

3. RESULTS AND DISCUSSION

3.1. PARTICLE CHARACTERIZATION

LNPs were prepared using microfluidic techniques, which allowed precise control over particle size and encapsulation. The prepared LNP formulations were characterized on both Day 1 shown in Table 3.1 and Figure 3.1 and Day 7 and Figure 3.2 shown in Table 3.2 post-synthesis, using dynamic light scattering (DLS) for size and polydispersity index (PI) and zeta potential measurements for surface charge stability.

The average particle sizes (Z-Average) ranged from 185.7 nm to 247.0 nm across formulations, with PPZ showing the smallest size (185.7 nm) and ALC the largest (247.0 nm). Polydispersity indexes (PIs) indicated homogeneity, with values ranging from 0.19 (PPZ) to 0.31 (C14), suggesting uniform particle distribution in each batch since they are around 0.3. Zeta potential measurements demonstrated near-neutral surface charges, with values between -1.321 mV (C12) and -1.568 mV (PPZ). These near-neutral charges facilitate prolonged circulation and reduced aggregation. Then Day 7 particle had a less than 10% increase and PI values remained between 0.23 and 0.32, indicating minor aggregation and sustained stability and homogeneity. Zeta potential measurements indicated stable surface charges, with minor fluctuations in potential. The consistency in particle size, PI, and zeta potential over time confirmed the stability of the LNP formulations, which is critical for clinical translation as it affects bioavailability and clearance rates in vivo.

Table 3.1. Day 1 of particle characterization

Day 1	ALC	C14	C12	MC3	PPZ
Polydispersity Index (PI) Homogeneity	0.25±0.03	0.31±0.05	0.20±0.02	0.28±0.04	0.19±0.01
Z-Average (nm)	247±7	216.9±8	185.7±6	191.8±5	187.2±4
Zeta (mV)	-1.546±0.235	-1.467±0.228	-1.321±0.729	-1.245±0.180	-1.568±0.860

Table 3.2. Day 7 of particle characterization

Day 7	ALC	C14	C12	MC3	PPZ
Polydispersity Index (PI) Homogeneity	0.32±0.04	0.32±0.07	0.29±0.04	0.23±0.06	0.30±0.03
Z-Average (nm)	265.4±10.1	258.9±11.3	198.3±9.5	217.5±8.6	199.3±7.4
Zeta (mV)	-1.238±0.564	-1.786±0.259	-1.238±0.799	-1.238±0.383	-1.200±0.180

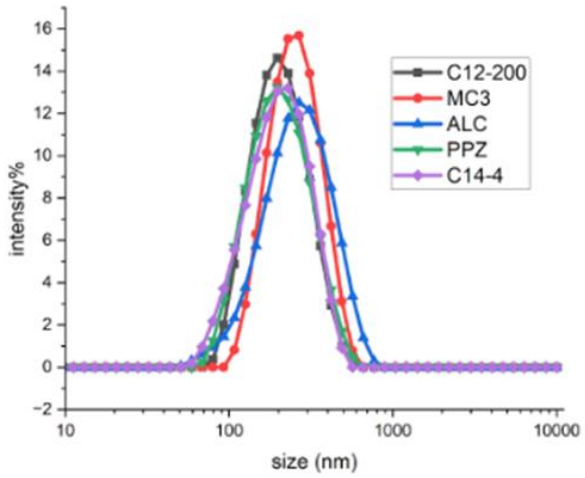

Figure 3.1. Day 1 LNP size distribution.

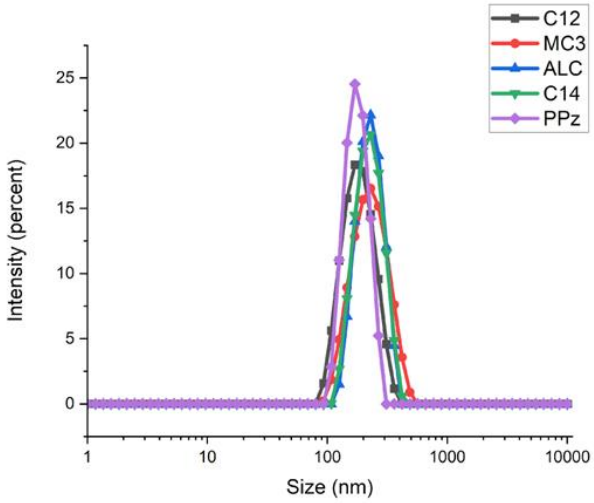

Figure 3.2. Day 2 LNP size distribution.

3.2. ENCAPSULATION EFFECIENCY

Encapsulation efficiency was assessed using gel electrophoresis and fluorescence-based assays. In the gel electrophoresis analysis, 0.5 µg/mL of mRNA was loaded per well, and the results demonstrated limited migration of encapsulated EGFP mRNA, indicating effective entrapment within the lipid nanoparticles (LNPs). In contrast, the free mRNA control migrated significantly, clearly distinguishing between encapsulated and unencapsulated mRNA. The gel image on Figure 3.3 further corroborates these findings, visually showcasing the separation between encapsulated and free mRNA. Fluorescence assays confirmed these results by detecting non-encapsulated mRNA at levels below the detection threshold, verifying successful encapsulation across all LNP formulations. High encapsulation efficiency, as demonstrated in these assays, is essential for therapeutic applications, as it ensures that the maximum possible amount of mRNA is delivered to target cells, which is critical for achieving effective therapeutic outcomes.

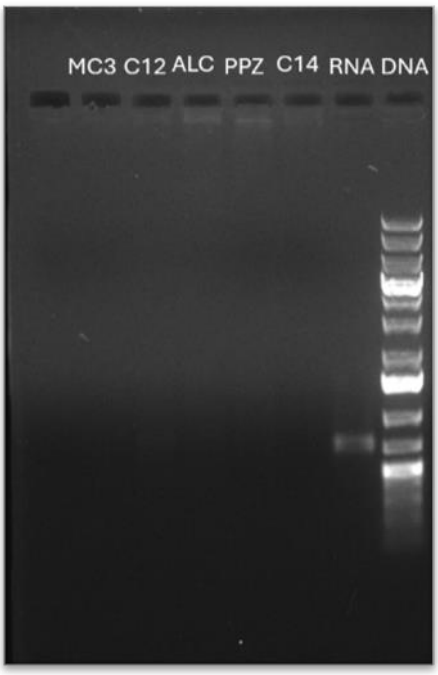

Figure 3.3. Gel Electrophoresis of LNP formulations with RNA and DNA ladder.

3.3. TRANSFECTION RESULTS

3.3.1. Fluorescence Microscopy. The transfection efficiency of EGFP mRNA-LNPs was initially assessed qualitatively via fluorescence microscopy. After 24 hours post-transfection, RAW 264.7 and MDA-MB-231 cells exhibited significant EGFP fluorescence. The fluorescence was localized within the cells, indicating successful internalization and expression of the EGFP mRNA payload. PPZ and C14 as shown in Figure 3.5, 3.6 and 3.7, 3.8 respectively formulations demonstrated the highest fluorescence intensity in both cell types, indicating superior mRNA delivery efficiency especially compared to the positive control lipofectamine as shown in Figure 3.4 and 3.9.

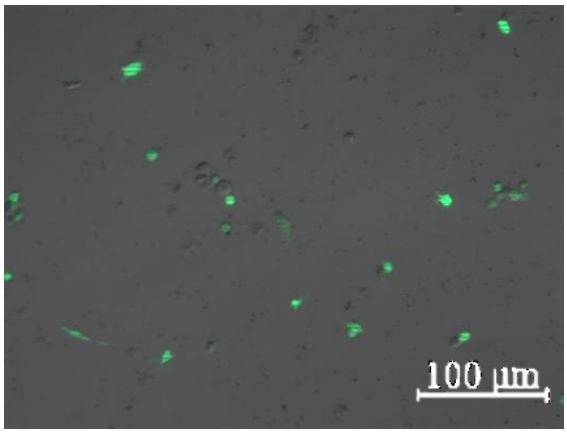

Figure 3.4 Fluorescent image of RAWW cell line with lipofectamine formulation

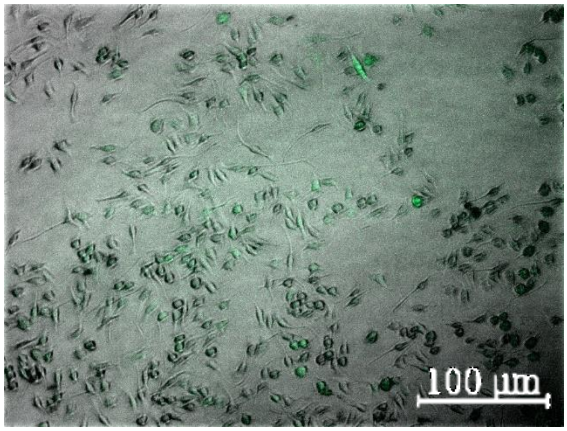

Figure 3.5 Fluorescent image of RAW cell line with PPZ formulation

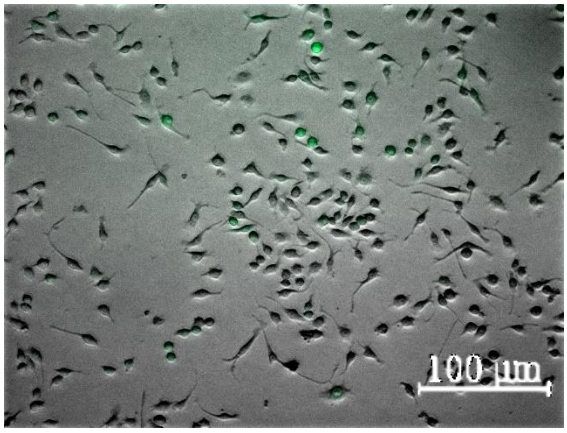

Figure 3.6 Fluorescent image of RAW cell line with C14 formulation

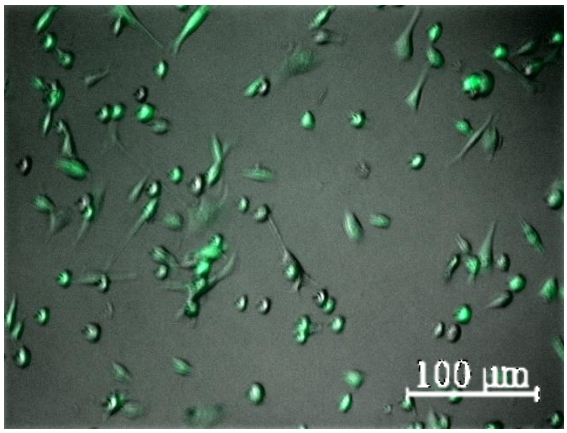

Figure 3.7 Fluorescent image of MDA-MB-231 cell line with C14 formulation

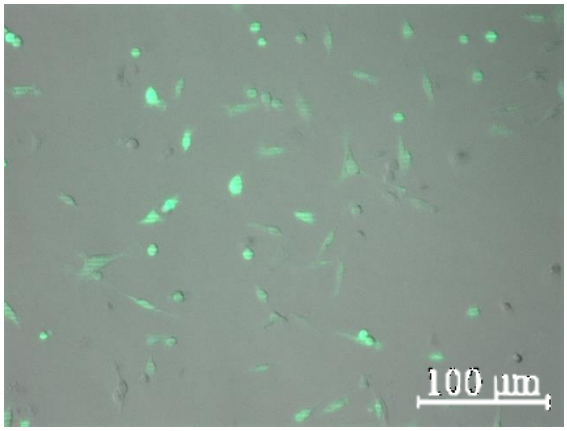

Figure 3.8 Fluorescent image of MDA-MB-231 cell line with PPZ formulation

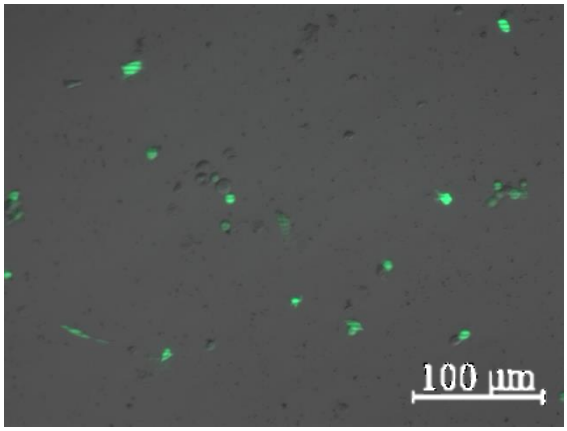

Figure 3.9 Fluorescent image of MDA-MB-231 cell line with lipofectamine

3.3.2. Flow Cytometry. Quantitative transfection efficiency was assessed using flow cytometry, allowing for the calculation of the percentage of EGFP-positive cells in each sample. In RAW 264.7 cells, the PPZ and C14 formulations shown in Figure 3.10, achieved the highest transfection efficiencies, with approximately 70% of cells showing EGFP expression. MDA-MB-231 cells, shown in Figure 3.11, showed a similar trend, with C14 and PPZ formulations achieving around 65% EGFP-positive cells. C12, showed moderate efficiencies, with approximately 50% EGFP-positive cells in RAW 264.7 shown in Figure 3.10. A visual comparing all the formulation for RAW and MDA-MB-231 cell lines is shown in Figure 3.12 and 3.13.

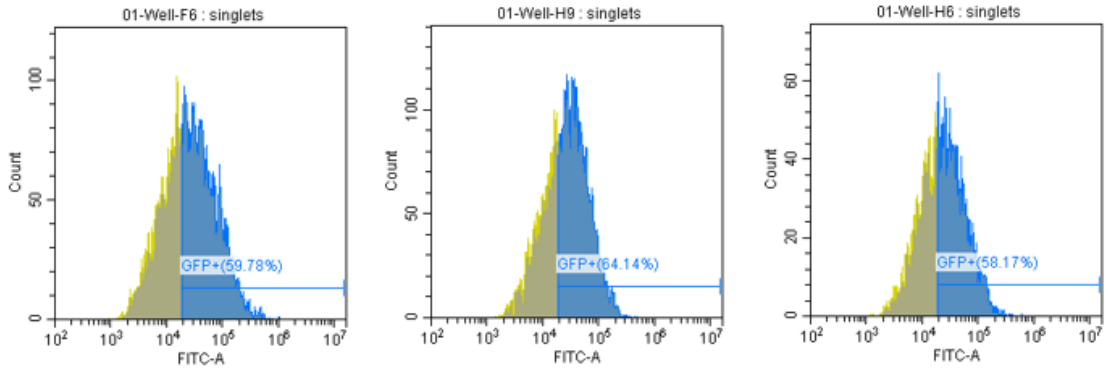

Figure 3.10 Flow cytometer FITC-A channel graph for RAW cell line with C14-4, C12, and PPZ formulation respectively.

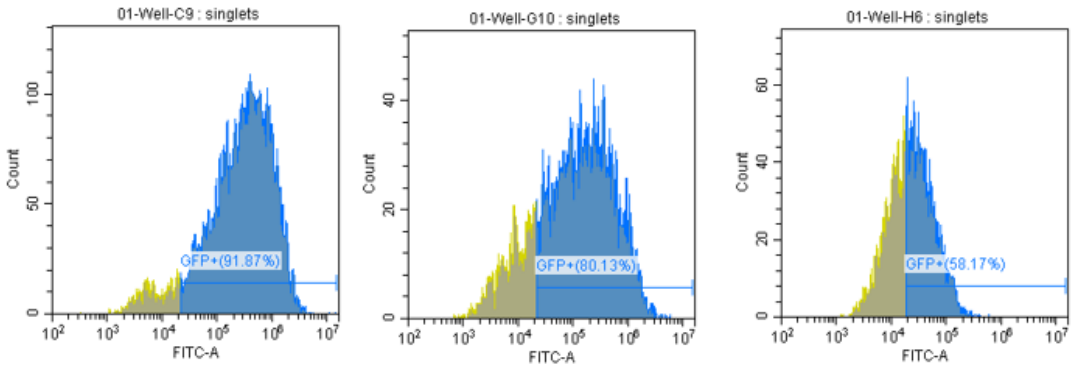

Figure 3.11. Flow cytometer FITC-A channel graph for MDA-MB-231 cell line with C14-4, PPZ, and lipofectamine formulation respectively.

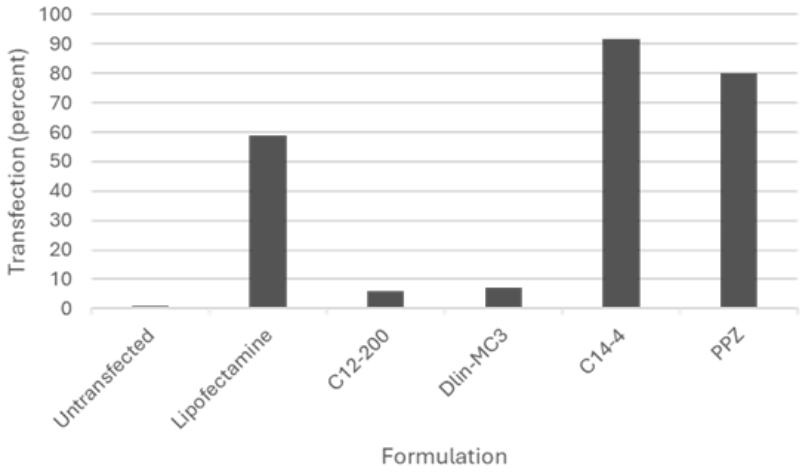

Figure 3.12 Flow cytometer transfection for MDA-MB-231 cell line with various formulations

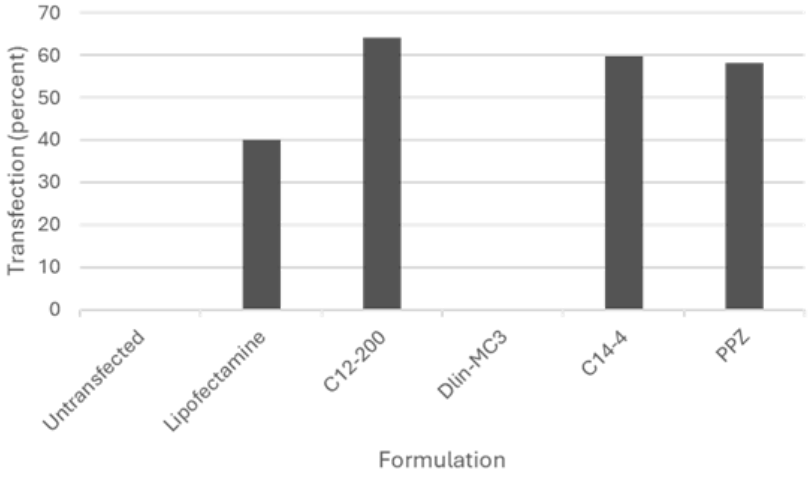

Figure 3.13: Flow cytometer transfection for RAW cell line with various formulations.

4. CONCLUSION

This study demonstrates the effectiveness of ionizable lipid nanoparticles (LNPs) as a nonviral platform for mRNA delivery, showcasing high encapsulation efficiencies, stable particle characteristics, and significant transfection efficiency in RAW 264.7 and MDA-MB-231 cell lines. Among the formulations tested, those containing PPZ and C14 lipids were most successful, achieving transfection rates of approximately. PPZ and C14 formulations emerged as the most promising candidates with transfection of over 80% in MDA-MB-231 and 50% in RAW 267.7, and higher than the positive control The stability of these LNP formulations over a week without substantial aggregation or changes in particle size or zeta potential with a size increase of less than 10% and PI around or under 0.3 is a promising indicator for the clinical viability of these particles, making them suitable candidates for applications in gene therapy, cancer treatment, and vaccine development.

To further improve targeting and therapeutic efficacy, future research should explore the following areas, using therapeutic mRNA, attaching targeting moieties, such as monoclonal antibodies, to the LNP surface could enhance cell-specific delivery, reducing off-target effects and improving therapeutic outcomes. By conjugating antibodies specific to cell-surface receptors on target cells, LNPs could selectively bind and deliver their payload to specific tissues, such as tumors or immune cells. For example, antibodies targeting cancer-specific markers (e.g., HER2 for breast cancer) could be conjugated to LNPs, guiding the particles to selectively deliver mRNA to cancerous cells while minimizing uptake by healthy cells. This targeted approach could

be beneficial in reducing the required dosage and minimizing side effects in cancer treatments.

Expanding the scope of these findings to in vivo models would provide insights into the biodistribution, pharmacokinetics, and pharmacodynamics of these LNPs in a living system. In vivo studies could assess the circulation time, clearance rates, and tissue-specific accumulation of each LNP formulation, as well as evaluate the immune response and any potential toxicity. This would be particularly useful for identifying formulations with optimal safety profiles and therapeutic effectiveness for future clinical applications. Additionally, animal models could be used to study the efficacy of these LNPs in delivering therapeutic mRNA for specific diseases, such as cancer or genetic disorders, further validating their potential in real-world therapeutic contexts.

To further refine the efficiency and versatility of LNPs, expanding the lipid library to include a broader range of ionizable and helper lipids could offer new avenues for optimization. Lipids with varied head groups, linkers, and tail structures could be screened to identify formulations with enhanced stability, cell uptake, and endosomal escape properties. A comprehensive lipid library, possibly including novel lipids engineered to improve encapsulation efficiency and reduce immunogenicity, could support the development of LNPs tailored for specific applications, such as delivering mRNA, siRNA, or CRISPR components. High-throughput screening of these lipid combinations would allow rapid identification of optimized formulations that maintain structural integrity and show enhanced delivery capabilities.

The findings of this study underscore the versatility and potential of LNP-based mRNA delivery systems, particularly for applications requiring high transfection

efficiency and stability. By integrating strategies such as antibody conjugation for targeted delivery, in vivo validation, and a broadened lipid library, future research can address remaining challenges and unlock the full therapeutic potential of LNPs. This approach has the potential to accelerate the development of next-generation therapies, including targeted cancer treatments, gene therapies, and vaccines, ultimately improving patient outcomes across a range of diseases.

APPENDIX

Excel Sheet for the calculations of the amount of lipids for ALC0315

ALC0315									
mRNA:ion	1:10 wt/wt								
	mol ratio	mol wt		total moles		0.208796			
ALC0315	50	766.3	0.104398	80	800	25	32		
DSPC	10	790.2	0.02088	16.49902	164.9902	4	41.24755		
chol	38.5	386.4	0.080386	31.06126	310.6126	25	12.4245		
PEG2000	1.5	2810.4	0.003132	8.801984	88.01984	12.5	7.041587		
Mal	0.5	4241	0.001044	4.427509	44.27509	10	4.427509	97.14115	vol
				1x	10x	conc	vol	1402.859	eth vol
							10x vol	1500	

BIBLIOGRAPHY

Akanda, M., Mithu, M. S. H., & Douroumis, D. Solid lipid nanoparticles: An effective lipid-based technology for cancer treatment. Journal of Drug Delivery Science and Technology, 86, 2023, 104709. https://doi.org/10.1016/j.jddst.2023.104709.

Augustine, R., Hasan, A., Primavera, R., Wilson, R. J., & Kevadiya, B. D. Cellular uptake and retention of nanoparticles: Insights on particle properties and interaction with cellular components. Materials Today Communications, 25, 2020, 101692. https://doi.org/10.1016/j.mtcomm.2020.101692.

Cetin, B., Erendor, F., Eksi, Y. E., Sanlioglu, A. D., & Sanlioglu, S. Gene and cell therapy of human genetic diseases: Recent advances and future directions. Journal of Cellular and Molecular Medicine, 28, 2024, e70056. https://doi.org/10.1111/jcmm.70056.

Giannopoulos-Dimitriou, A., Saiti, A., Petrou, A., Vizirianakis, I. S., & Fatouros, D. G. Liposome stability and integrity. In S. G. Antimisiaris (Ed.), Liposomes in Drug Delivery, Academic Press, 2024, 89–121. https://doi.org/10.1016/B978-0-443-15491-1.00022-5.

Haque, M. A., Shrestha, A., Mikelis, C. M., & Mattheolabakis, G. Comprehensive analysis of lipid nanoparticle formulation and preparation for RNA delivery. International Journal of Pharmaceutics X, 8, 2024, 100283. https://doi.org/10.1016/j.ijpx.2024.100283.

Hope, M. J., Bally, M. B., Mayer, L. D., Janoff, A. S., & Cullis, P. R. Generation of multilamellar and unilamellar phospholipid vesicles. Chemistry and Physics of Lipids, 40(2–4), 1986, 89–107. https://doi.org/10.1016/0009-3084(86)90065-4.

Jiang, H., Weng, X., & Li, D. A novel microfluidic flow focusing method. Biomicrofluidics, 8(5), 2014, 054120. https://doi.org/10.1063/1.4899807.

Jürgens, D. C., Deßloch, L., Porras-Gonzalez, D., et al. Lab-scale siRNA and mRNA LNP manufacturing by various microfluidic mixing techniques – an evaluation of particle properties and efficiency. OpenNano, 12, 2023, 100161. https://doi.org/10.1016/j.onano.2023.100161.

Kauffman, K. J., Dorkin, J. R., Yang, J. H., et al. Optimization of lipid nanoparticle formulations for mRNA delivery in vivo with fractional factorial and definitive screening designs. Nano Letters, 15(11), 2015, 7300–7306. https://doi.org/10.1021/acs.nanolett.5b02497.

Kumar, V., Barwal, A., Sharma, N., et al. Therapeutic proteins: Developments, progress, challenges, and future perspectives. 3 Biotech, 14, 2024, 112. https://doi.org/10.1007/s13205-024-03958-z.

Liu, Y., Cheng, C., Prud'homme, R. K., & Fox, R. O. Mixing in a multi-inlet vortex mixer (MIVM) for flash nano-precipitation. Chemical Engineering Science, 63(11), 2008, 2829–2842. https://doi.org/10.1016/j.ces.2007.10.020.

Lopes, C., Cristóvão, J., Silvério, V., Lino, P. R., & Fonte, P. Microfluidic production of mRNA-loaded lipid nanoparticles for vaccine applications. Expert Opinion on Drug Delivery, 19(10), 2022, 1381–1395. https://doi.org/10.1080/17425247.2022.2135502.

Maeki, M., Okada, Y., Uno, S., et al. Mass production system for RNA-loaded lipid nanoparticles using piling up microfluidic devices. Applied Materials Today, 31, 2023, 101754. https://doi.org/10.1016/j.apmt.2023.101754.

Mendonça, M. C. P., Kont, A., Kowalski, P. S., & O'Driscoll, C. M. Design of lipid-based nanoparticles for delivery of therapeutic nucleic acids. Drug Discovery Today, 28(3), 2023, 103505. https://doi.org/10.1016/j.drudis.2023.103505.

Minskaia, E., Galieva, A., Egorov, A. D., et al. Viral vectors in gene replacement therapy. Biochemistry Moscow, 88, 2023, 2157–2178. https://doi.org/10.1134/S0006297923120179.

Mueller, C., Bialk, P., & Cox, R. M. Delivery of large genome editing nucleic acid payloads using lipid nanoparticles. Nature Biotechnology, 42(8), 2024, 1124–1133. https://doi.org/10.1038/s41587-024-01635-y.

Patel, S., Ashwanikumar, N., Robinson, E., et al. Naturally occurring ionizable lipid nanoparticles for nucleic acid delivery. ACS Nano, 15(4), 2021, 10778–10792. https://doi.org/10.1021/acsnano.1c02782.

Pardi, N., Hogan, M. J., Porter, F. W., & Weissman, D. mRNA vaccines: A new era in vaccinology. Nature Reviews Drug Discovery, 17(4), 2018, 261–279. https://doi.org/10.1038/nrd.2017.243.

Sabnis, S., Kumarasinghe, E. S., Salerno, T., et al. A novel ionizable lipid for effective mRNA delivery. Molecular Therapy, 26(5), 2018, 1509–1519. https://doi.org/10.1016/j.ymthe.2018.03.011.

Sahay, G., Querbes, W., Alabi, C. A., et al. Efficiency of siRNA delivery by lipid nanoparticles is limited by endocytic recycling. Nature Biotechnology, 31(7), 2013, 653–658. https://doi.org/10.1038/nbt.2614.

Schmidt, M. J., Tiwari, S., Chi, C., & Ghildyal, R. Factors influencing nanoparticle interaction with cells for enhanced delivery efficiency. Pharmaceutics, 15(3), 2023, 713. https://doi.org/10.3390/pharmaceutics15030713.

Shim, G., Lee, S., & Kim, Y. B. Advances in polymeric nanoparticles for mRNA delivery. Advanced Drug Delivery Reviews, 187, 2024, 114592. https://doi.org/10.1016/j.addr.2023.114592.

Teo, P. Y., Zhu, H., & Zhang, Y. Lipid nanoparticles: Insights into cell membrane interactions. Advanced Materials, 33(17), 2024, 2109097. https://doi.org/10.1002/adma.202109097.

Vogus, D. R., Krishnamurthy, V. R., Desai, T. A., & Mitragotri, S. Nanoparticle targeting strategies: From functionalization to guided navigation. Nature Nanotechnology, 17(1), 2024, 3–17. https://doi.org/10.1038/s41565-023-01389-8.

Yanez, M., Nold, T., & Voit, C. E. Comparison of hydrodynamic mixing techniques for lipid nanoparticle synthesis. Bioconjugate Chemistry, 34(5), 2023, 1132–1142. https://doi.org/10.1021/acs.bioconjchem.3c00258.

VITA

Lavanya Bhargava was born in Alwar, India, and moved to St. Louis, Missouri, in the sixth grade. She attended the Missouri University of Science and Technology, where she graduated with a Bachelor of Science in Chemical Engineering, with an emphasis in Biochemical Engineering, in May 2023. During her undergraduate studies, she completed a hands-on manufacturing internship at Royal Oak, focusing on optimizing production processes, and conducted biochemical research under Dr. Hu Yang, contributing to projects on lipid-based nanoparticles for gene and drug delivery. She continued her academic journey at Missouri S&T, earning a Master of Science in Chemical Engineering in December 2024. Beyond her academic achievements, Lavanya was highly engaged in campus life and took on leadership roles across diverse organizations. She served as Chief Financial Officer of the Underwater Robotics team, Risk Management Chair for Delta Omicron Lambda and Lambda Sigma Pi within the Greek Independent Council, External Finance Chair for the Student Activity Finance Board, Secretary of Trap and Skeet, and Treasurer of the Club Sports Council. Her active involvement reflects her dedication to building a well-rounded skill set in both technical and leadership arenas, preparing her for impactful contributions in the field of chemical engineering.